The Meteoritical Society

Meteoritics & Planetary Science 55, Nr 8, E1–E20 (2020)
doi: 10.1111/maps.13556

Check for updates

Electronic-Only Article

The surprising thermal properties of CM carbonaceous chondrites

C. P. OPEIL [1]*, D. T. BRITT [2,3], R. J. MACKE [4], and G. J. CONSOLMAGNO[4]

[1]Department of Physics, Boston College, 140 Commonwealth Ave., Chestnut Hill, Massachusetts 02467, USA
[2]Department of Physics, University of Central Florida, 4111 Libra Dr., Orlando, Florida 32816, USA
[3]The Center of Lunar and Asteroid Surface Science, 12354 Research Pkwy Suite 214, Orlando, Florida 32826, USA
[4]Vatican Observatory, V-00120 Vatican City State
*Corresponding author. E-mail: opeil@bc.edu

(Received 27 December 2019; revision accepted 17 July 2020)

Abstract–Measurements of the low-temperature thermodynamic and physical properties of meteorites provide fundamental data for the study and understanding of asteroids and other small bodies. Of particular interest are the CM carbonaceous chondrites, which represent a class of primitive meteorites that record substantial chemical information concerning the evolution of volatile-rich materials in the early solar system. Most CM chondrites are petrographic type 2 and contain anhydrous minerals such as olivine and pyroxene, along with abundant hydrous phyllosilicates contained in the meteorite matrix interspersed between the chondrules. Using a Quantum Design Physical Property Measurement System, we have measured the thermal conductivity, heat capacity, and thermal expansion of five CM2 carbonaceous chondrites (Murchison, Murray, Cold Bokkeveld, Northwest Africa 7309, Jbilet Winselwan) at low temperatures (5–300 K) which span the range of possible surface temperatures in the asteroid belt and outer solar system. The thermal expansion measurements show a substantial and unexpected decrease in CM2 volume as temperature increases from 210 to 240 K followed by a rapid increase in CM2 volume as temperature rises from 240 to 300 K. This transition has not been seen in anhydrous CV or CO carbonaceous chondrites. Thermal diffusivity and thermal inertia as a function of temperature are calculated from measurements of density, thermal conductivity, and heat capacity. Our thermal diffusivity results compare well with previous estimates for similar meteorites, where conductivity was derived from diffusivity measurements and modeled heat capacities; our new values are of higher precision and cover a wider range of temperatures.

INTRODUCTION

Characterizing the thermal properties of asteroids is fundamental for a range of planetary exploration applications including modeling asteroidal orbital response to the space environment; the potential for degradation from thermal shock; and for planning the interactions of spacecraft, robotic or crewed, with asteroid surfaces (Bottke et al. 2006; Vokrouhlický et al. 2015).

The thermal and mechanical properties of asteroidal materials are important in modeling the response of their surfaces to impact cratering and the formation of asteroid regolith (Delbó et al. 2014; Hazeli et al. 2018; El Mir et al. 2019; Ravaji et al. 2019). Asteroid surface temperatures also determine the thermal radiation environment within which exploration instruments and astronauts must work. Excessive thermal radiation can blind or damage detectors, affect the thermal balance of spacecraft, and perturb the operation of the spacecraft's thermal radiators. Another critical process is the weakening and degradation of asteroidal boulders from thermal shock (Molaro et al. 2017). This process is critically dependent on the compositionally specific response of asteroidal (thus meteorite) materials to thermal input and thus their thermal properties.

Table 1. Measured meteorite bulk density, ρ, calculated Debye temperature, Θ_D, and effective molar mass are shown. Bulk density measurements are comparable with other CM2 literature values as measured by Britt and Consolmagno (2003), Consolmagno et al. (2008), and Macke et al. (2011). Porosity data are referenced from Macke (2010)[a] and R. J. Macke, unpublished data.[b] They reflect population averages and standard deviations, as porosities were not measured for the individual specimens in this study.

Meteorite	ρ (kg m^{-3})	Θ_D (K)	Effective molar mass (g mol^{-1})	Porosity (%)
Cold Bokkeveld	2310 ± 20	530.2	46.30	15.0 ± 3.4[a]
Jbilet Winselwan	2040 ± 20	549.8	46.45	26.4 ± 0.8[b]
Murchison	2320 ± 20	550.6	49.20	22.1 ± 2.2[a]
Murray	2210 ± 20	556.5	49.18	20.8 ± 2.0[a]
NWA 7309	2300 ± 20	541.5	49.95	No data

Thermal properties are also essential in the modeling of meteor brightness as a function of the meteor initial size and speed, which provides us further information on material derived from the asteroid belt.

The Yarkovsky and YORP effects on asteroid orbital and spin perturbations depend on the thermal inertia, Γ defined as $(\rho\ c_p\ \kappa)^{1/2}$, where ρ is the density of the material, c_p is the heat capacity, and κ is the thermal conductivity. The thermal evolution of the interiors of asteroids and of comets, satellites, and other volatile-rich bodies depends on the thermal diffusivity, D_T defined as $(\kappa\ \rho^{-1}\ c_p^{-1})$, the ratio of the thermal conductivity to the volumetric heat capacity, and it is a critical input into accurate models of asteroid volatile release and retention.

Our previous work has shown conclusively that meteorite thermal properties are controlled both by the mineralogical composition of the sample and by its physical state (Opeil et al. 2010, 2012). In particular, we have demonstrated that the thermal conductivity of volatile-rich carbonaceous chondrites is half that of most ordinary chondrites or anhydrous carbonaceous chondrites, while metal-rich enstatite chondrites are much more conductive. Notably, for several ordinary chondrites, the thermal conductivity is significantly different when measured in different directions, across different faces of the same cut sample, indicating that chemistry or mineralogy is not the only significant factor. The nature and orientation of internal cracks in the sample obviously play an important role. Indeed, in our data, we see a trend suggesting that conductivity is related to the inverse of the porosity of the sample. In Table 1, we include the bulk porosity data for the four of the five meteorites used in this study, which range from 15.0% to 26.4%. The porosities shown in Table 1 represent population averages and are not measured for the individual meteorite specimens used in this study (Macke 2010).

But most importantly, our data show that the thermal properties of meteorites are a strong function of temperature at the low temperatures appropriate to material in the outer solar system. While most pure minerals have been measured in the lab at 300 K, the equilibrium temperature of material in the asteroid belt is approximately 225 K; at Jupiter, it is 110 K, at Saturn 80 K, and can be 40 K or colder in the region of trans-Neptunian objects. Furthermore, these are daytime temperatures; for slowly rotating objects, the temperature of the nighttime surface will be much lower —a function of the object's spin rate and of its thermal inertia, which itself is a function of temperature.

We have been systematically measuring the thermal properties of samples of the major meteorite groups. A group of particular interest are the CM2 carbonaceous chondrites. They represent possible analogs of primitive, volatile-rich asteroids which are major exploration targets because of their potential as a feedstock source for in situ resource utilization (ISRU), as well as a unique mineralogical probe into the evolution of volatile-rich materials in the early solar system. Most CM2 chondrites contain both anhydrous minerals such as olivine and pyroxene, along with abundant hydrous phyllosilicates (Brearley 2006; Weisberg et al. 2006). We have measured the thermal conductivity, heat capacity, and thermal expansion of five CM2 carbonaceous chondrites (Murchison, Murray, Cold Bokkeveld, Northwest Africa [NWA] 7309, Jbilet Winselwan) at low temperatures (5–300 K), which span the range of possible surface temperatures in the asteroid belt.

EXPERIMENTAL METHODS

The cryogenic measurements of heat capacity, thermal conductivity, and thermal expansion were made using a Quantum Design Physical Property Measurement System (QD-PPMS) at Boston College. This system controls temperature within the range of 2–400 K and with an adsorption pump provides a sample vacuum environment of $p \leq 10^{-6}$ Torr (~10^{-4} Pa) for thermal isolation. Heat transfer in

porous media can be significantly affected by gases in the pores; however, thermal properties of porous media are not dependent on ambient gas pressure if $p < 10^{-3}$ Torr (~10^{-1} Pa; Fujii and Osako 1973; Matsui and Osako 1979). Thus, sample measurements at a pressure below 10^{-3} Torr can be considered low enough to estimate thermal properties in planetary space. Samples of the meteorites were cut from the interiors of their main mass to minimize any effect of surface weathering and/or ablative alteration. Geometric shapes were obtained using a slow speed diamond saw and subsequently polished with 400 and 1500 grit SiC paper. Bulk density measurements, ρ, were made by the Archimedes method and by mass/volume measurements on parallelepiped sample shapes. Bulk density values are listed in Table 1. These values are consistent with previous bulk density measurements made on similar CM2 samples (Britt and Consolmagno 2003; Macke 2010; Macke et al. 2011).

Heat capacity measurements were made on samples approximately $1 \times 3 \times 3$ mm in size with a mass of 20–50 mg. Samples were thermally connected with the sapphire heat capacity platform with Apiezon N grease. The QD-PPMS uses a hybrid adiabatic relaxation heat capacity method that combines both high accuracy and a robust error analysis. Further details of the QD-PPMS heat capacity measurements and sample preparation techniques are provided by Lashley et al. (2003). Measurements of both single crystal Cu and Pyrex 7740 standards were performed on the heat capacity puck to confirm current thermometer calibrations. Data were taken, with approximately 75 measurements per sample, using a log-T (2–300 K) spacing to allow for a higher point density at low temperatures.

As with our previous work (Opeil et al. 2010), thermal conductivity measurements were performed using the thermal transport option (TTO) of the QD-PPMS that allows thermal conductivity measurements (W m^{-1} K^{-1}) across a broad temperature range (2–390 K). Thermal conductivity data are obtained while maintaining a pressure of $p \leq 10^{-6}$ Torr by sending a heat pulse, Q, from one end of the sample to the other while monitoring a time-dependent temperature signature as Q is transferred to the cold finger. A thorough description of this measurement technique is provided by Dilley et al. (2002). Accuracy of the current measurements and thermometer calibrations were confirmed using both a Quantum Design Ni-alloy and Pyrex 7740 standards. After cutting rectangular parallelepiped samples of approximately $2 \times 2 \times 12$ mm, each with a mass of ~0.2 to 0.5 g, each end was attached to an Au-coated, oxygen-free, high-conductivity Cu disk with Ag epoxy (EPO-TEK H20E from Epoxy Technology) thermally anchoring the calibrated Cernox thermometers, heater, and cold finger to the sample, see Fig. 1.

Fig. 1. Thermal conductivity sample (NWA 7309) attached with Ag epoxy and mounted on QD-PPMS TTO measurement puck. The Lincoln penny is added as a scale reference. (Color figure can be viewed at wileyonlinelibrary.com.)

Thermal expansion/contraction measurements were performed using a capacitive dilatometer to determine what volumetric or density changes might arise between ambient and cryogenic temperatures. Additionally, this measurement is designed to determine if these meteoritic materials experience any sudden expansion/contraction as a function of temperature. The dilatometer used in these experiments (Fig. 2) was manufactured at Los Alamos National Laboratory and originally intended to detect crystallographic and magnetic phase transitions on single and polycrystal alloys, but is applicable for any solid material between 2 and 300 K. Meteoritic samples with dimensions of approximately $3 \times 4 \times 4$ mm were placed in a capacitive dilatometer where the expansion/contraction of a sample is measured by allowing one plate of a parallel-plate capacitor to follow the linear dimensional change it undergoes as a function of temperature or field. These changes translate into a variation in the dilatometer capacitor plate separation as a function of temperature or applied magnetic field.

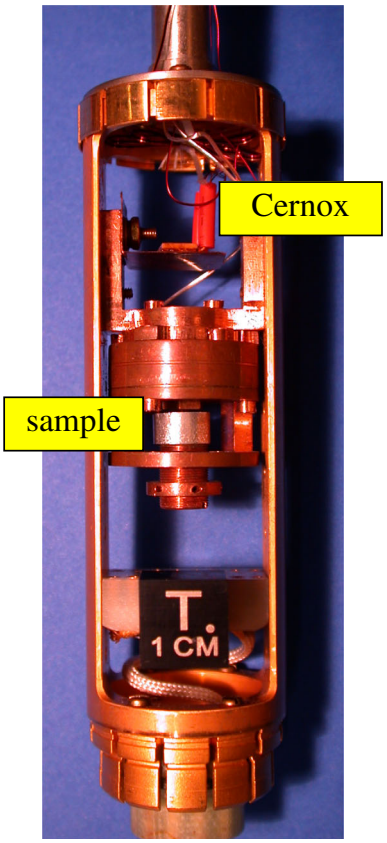

Fig. 2. Capacitive dilatometer with a calibrated Cernox thermometer shown above the sample.

For an ideal parallel-plate capacitor in vacuum, the relationship between the measured capacitance, C, and the gap, d, between the pair of capacitor plates is $d = \epsilon_o$ A C^{-1} where ϵ_o is the permittivity of free space and A is the area of the capacitor plates. The capacitance of the dilatometer is measured by an Andeen-Hagerling, AH-2550A Ultra-precision Capacitance Bridge with a resolution of 0.8 aF while averaging 10^3 measurements per data point. Temperature is monitored by a calibrated Cernox thermometer (CX-050-BG-HT) close to the sample. Data were taken with a cooling/warming rate of 0.25 K min^{-1}. Dilatometer calibrations were performed using an Al polycrystal (99.999%, Alfa Aesar, Puratronic) cylinder and are comparable with the results of Kroeger and Swenson (1977). Additional details on the dilatometer used for these measurements are provided by Schmiedeshoff et al. (2006).

DATA

Thermal Conductivity

Thermal conductivity, κ, is an intrinsic, temperature-dependent property of a material and describes the transport of heat energy through a body of mass resulting from a temperature gradient across the sample (Sass et al. 1971). Previous studies on natural terrestrial minerals and rocks at high temperature (293–873 °C) allow analysis of the temperature dependence of κ by the simple relation $\kappa = 1/(A + BT)$, where A and B are constants determined by the particular sample type (Cermak and Rybach 1982; Vosteen and Schellschmidt 2003).

Phonons are a crystal's method of moving thermal energy. At lower temperatures (2–300 K), it is necessary to consider the heat energy transported in materials and thermal conductivity, κ, as a combination of both free electrons (κ_e) and phonons (κ_{ph}); thus, the total thermal conductivity can be represented as $\kappa_{tot} = \kappa_e + \kappa_{ph}$ (Levy 1968; Cermak and Rybach 1982; Grimvall 1999; Hofmeister et al. 2007; Xiong and Zhang 2019). Since the majority of the crystalline phyllosilicates in CM2 matrices are ferroan serpentine group minerals, where the generalized compositions can be expressed as $(Fe, Mg)_3$ $SiO_5(OH)_5$, as described by McSween (1987), we give particular consideration to their insulating characteristics. As with many metallic oxides, the energy gap between valence and conduction bands can be on the order of ~3 eV, essentially forbidding electrons from flowing freely in the material (Rao and Rao 1970). Since the chemical composition of CM2 carbonaceous chondrites allows for few free electrons (Browning et al. 1996), one can assume $\kappa_e \sim 0$ and thermal conductivity can be approximated entirely by phonon–phonon collisions and phonon movement in the material, thus $\kappa_{tot} \sim \kappa_{ph}$.

For insulating solid materials, thermal conductivity can be modeled by the equation $\kappa_{ph} = (n\ c_p\ v_{ph}\ \lambda_{ph})/3$, where c_p is the volumetric specific heat, v_{ph} is the phonon velocity (or sound velocity) in the material, n is the number of moles per unit volume, and λ_{ph} is the mean free path of a phonon in the sample (Rosenberg 1992). Sound velocity, v_{ph}, can be considered to be relatively constant or slowly varying across temperature, in contrast to the strong temperature dependence of c_p and $\lambda_{ph.}$ It is understood according to Debye theory for all materials that c_p reaches a constant value at high temperatures ($T > 300$ K) and at low temperatures ($T < 100$ K) specific heat varies as T^3 as described by Turton (2005). Therefore, the temperature-dependent behavior of κ_{ph} is directly proportional to the product of c_p and λ_{ph}.

The phonon mean free path, λ_{ph}, describes the average distance a phonon travels within the sample before its motion is noticeably altered by collisions (or scattering) with defects, material voids, grain boundaries, the sample boundary, or another phonon. Frequent scattering lowers the value of λ_{ph}. At low

temperatures, (e.g., $T \leq 100$ K), the scarcity of thermal energy allows few activated phonons, so there is little statistical chance of phonon–phonon interaction. Furthermore, given that $E = h\ c/\lambda$, where E is energy, h is Planck's constant, c is the speed of light, and λ is wavelength, phonons with low energy have large wavelengths and this limits their ability to scatter off impurities or defects in the sample. Thus, in the low-temperature regime, the thermal conductivity increases roughly as T^3 (as does c_p) until phonon scattering becomes statistically significant and λ_{ph} begins to decrease. As temperature increases ($T > 100$ K), phonon scattering results in a change in the slope of κ_{ph} where a broad maximum develops in the curve. This maximum is related to the increased number of activated and higher energy phonons possessing shorter wavelengths, which allow more frequent interactions with defects, grain boundaries, and material voids.

Allowing that CM2 meteorites are conglomerates of mafic silicate and phyllosilicate materials (Wood 1967; McSween 1979; Rubin et al. 2007), it can be assumed that impurity-driven scattering dominates in these samples, since on an atomic level, they are highly disordered. Thus, for $200 < T < 300$ K, one predicts that due to sample disorder and impurity-driven scattering, the thermal conductivity will fall as T^{-1} which follows the analysis of Cermak and Rybach (1982) at higher temperatures. To summarize this behavior, one expects the thermal conductivity in a typical insulating material to rise sharply as temperature increases from 0 K to some maximum value between 100 and 300 K, followed by a T^{-1} decrease as temperature increases. Variations in the behaviors of κ_{ph} after its maxima are determined by the material composition, porosity, density contrasts, grain boundaries, and the thermodynamic equilibrium reached by the product of c_p and λ_{ph}.

The thermal conductivity data from the five CM2 meteorite samples are shown in Fig. 3. It is noted that overall for this sample group $\kappa < 1.2$ (W m^{-1} K^{-1}) with Murchison only achieving a value of $\kappa \sim 0.5$ (W m^{-1} K^{-1}) at the highest temperature. There is evidence of an increase in κ from the lowest temperatures to a distinct slope change at about 100 K for Cold Bokkeveld, Jbilet Winselwan, Murchison, and Murray. The NWA 7309 sample shows the onset of a weak low-temperature maximum in κ occurring a little lower at about 75 K and is followed by a slight decrease in κ magnitude, likely due to phonon scattering. The unusual variation in κ of NWA 7309 above 100 K is attributable to temperature-dependent changes in λ_{ph}. NWA 7309, Murchison, and Jbilet Winselwan reach a constant value as they approach room temperature. To make these thermal conductivity data available to other researchers, they were fit to a simple fourth order polynomial, $\kappa\ (T) = A + B\ T + C\ T^2 + D\ T^3 + E\ T^4$ where the coefficients A, B, C, D, and E are obtained by the least-squares fit and shown in Table 2. These thermal conductivity data are consistent with a disordered insulating material where significant phonon scattering results from interactions with defects, voids, grain boundaries, and other phonons. In fact, these results show evidence of a disordered crystalline solid (Stachurski 2011) to the degree that the phonon mean free path, λ_{ph}, reaches a constant value due to sample boundary scattering, and any rise in κ at $T > 250$ K is due to its proportionality with specific heat.

Heat Capacity

Specific heat capacity (c_p) is an intrinsic bulk property of a substance. In the absence of any phase change, it signifies the amount of heat energy necessary to raise the temperature of a certain mass of a material. This represents the amount of heat stored in the material's oscillating atomic movements, whose frequency and mode are temperature dependent. Chemical bonds can be treated as an oscillator whose fundamental frequency is determined by the elastic constant of that particular bond and the masses of the attached atoms. For a solid, no atomic bond is isolated but rather part of a larger crystal lattice; thus, these oscillations do not occur as individual bonds. Instead, the vibrations are expressed in frequency modes that are excited along preferred lattice directions.

The specific heat of most solids at room temperature and above reaches a similar constant value when their mass is expressed in molar units. This relationship was first expressed by Dulong and Petit in 1819 as noted by Kittel (1996) and Loehle et al. (2017). However, at lower temperatures ($T < 100$ K), specific heat drops rapidly as quantum processes become significant. The low-temperature behavior of homogeneous crystals is described by the Einstein–Debye (E–D) model of specific heat. This model shows that the drop-off in specific heat capacity with temperature is proportional to T^3 and it is well established experimentally for isotropic homogeneous materials (Aschroft and Mermin 1976). Deviations from this low-temperature E–D model and analysis are attributable to crystal disorder and sample inhomogeneity, which impede or suppress certain vibrational modes that transport thermal energy.

The specific heat capacity measurements from 2 to 300 K for Murray, Murchison, NWA 7309, Cold Bokkeveld, and Jbilet Winselwan are shown in Fig. 4. These heat capacity data confirm the strong low-temperature dependence and indicate the high-temperature saturation behavior at $T > 250$ K. Similar

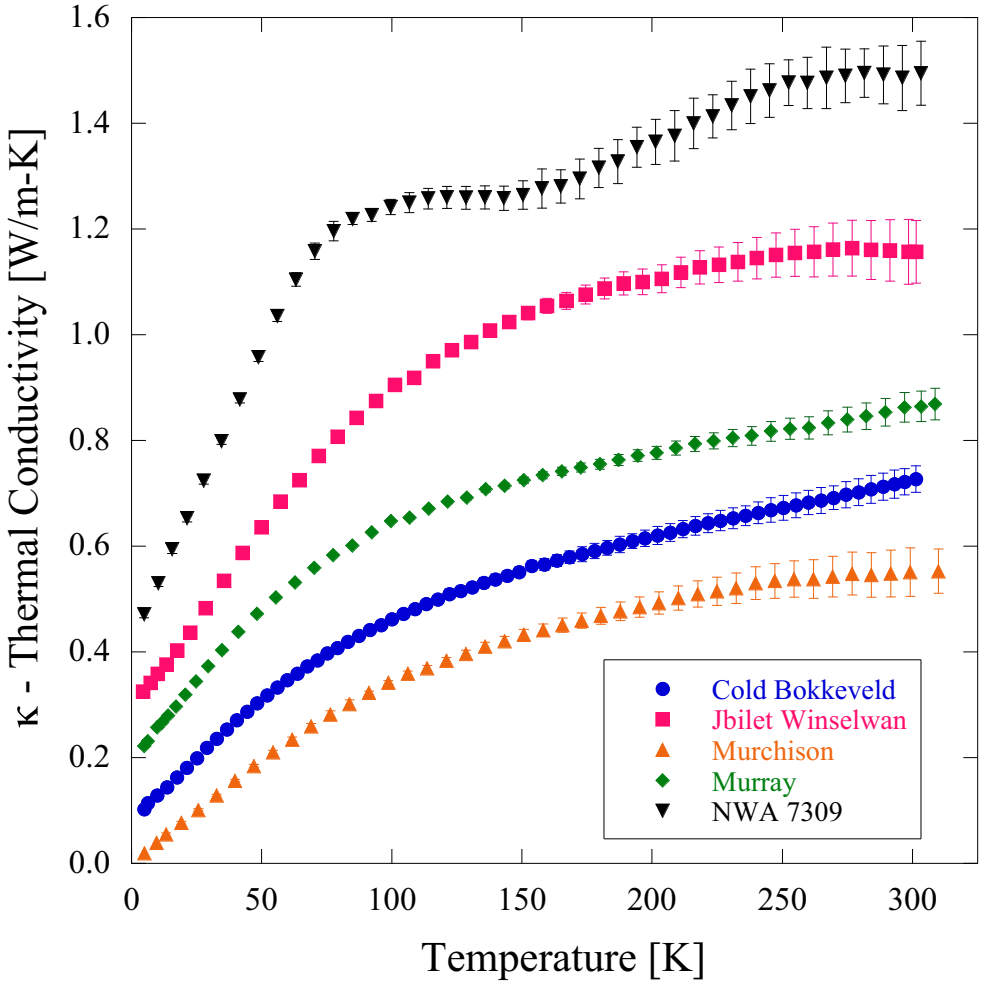

Fig. 3. Thermal conductivity (κ) versus temperature data are shown for five CM chondrite samples. The data are offset on the vertical axis by multiples of +0.1 W m^{-1} K^{-1} for clarity. Sample dimensions were ~2 × 3 × 10 mm (see Fig. 1) and measured with a cooling rate of 0.5 K min^{-1}. (Color figure can be viewed at wileyonlinelibrary.com.)

c_p temperature dependence is shown by Łuszczek and Wach (2014) in the analysis of NWA 6255 in a higher temperature range of 223–823 K. As expected in a conglomerate material with considerable crystalline disorder, no sharp peaks or evidence of phase transitions are indicated for any of the CM2 samples. In the high-temperature regime, slight differences among the curves are noted; NWA 7309 tends to flatten out more at a lower temperature than the four other samples.

The specific heat capacity data for $T \leq 25$ K were fit to the equation $c_p(T) = N\ T + P\ T^3$, where first-order term represents the low-temperature electronic portion of c_p and the cubic term represents the lattice contribution according to Debye theory. In order to compare data across the full temperature range ($T \leq 300$ K), they were fit to the Shomate formulation, $c_p(T) = a + b\ T + c\ T^2 + d\ T^3 + e\ T^{-2}$; the Haas–Fisher model, $c_p(T) = g + 2\ h\ T + j\ T^{-2} + k\ T^{-0.5} + m\ T^2$; and a simple fourth order polynomial, $c_p(T) = G + H\ T + J\ T^2 + L\ T^3 + M\ T^4$. Comparing the model fits, particularly at low temperature, it was determined that the simple fourth order polynomial fit yields the least error (Shomate 1954; Haas and Fisher 1976; Waples and Waples 2004; Vu et al. 2019).

The constants G, H, J, L, M, N, and P are obtained by the least-squares fit and are listed in Table 3. The data show that all samples conform to the general specific heat capacity behavior of materials across a temperature range of $2 < T < 300$ K, a strong temperature dependence at low temperature proportional to T^3 while at higher temperatures ($T > 250$ K), the samples achieve a constant heat capacity value. We note that if CM2 meteorites contain some metallic grains (particles of FeNi alloys) interspersed in the meteorite, these metallic particles are surrounded by an insulating

Table 2. For the thermal conductivity versus temperature data shown in Fig. 3, coefficients A, B, C, D, and E were calculated as a fit to the polynomial formula: $\kappa(T) = A + B\,T + C\,T^2 + D\,T^3 + E\,T^4$ for $T \leq 300$ K.

Meteorite	$A \times 10^{-2}$ (W m^{-1} K^{-1})	$B \times 10^{-3}$ (W m^{-1} K^{-2})	$C \times 10^{-5}$ (W m^{-1} K^{-3})	$D \times 10^{-8}$ (W m^{-1} K^{-4})	$E \times 10^{-11}$ (W m^{-1} K^{-5})
Cold	−3.008	5.948	−2.576	5.802	−4.654
Bokkeveld Jbilet	−3.555	9.024	−3.185	4.063	−0.463
Winselwan Murchison	−1.171	5.067	−1.936	4.142	−4.098
Murray	−2.081	7.855	−4.271	11.463	−11.410
NWA 7309	−8.842	20.839	−17.462	66.050	−88.770

phyllosilicate matrix effectively isolating free electron movement. The constant heat capacity values achieved at higher temperatures ($T > 250$ K) are similar for all CM2 samples studied and any differences are indicative of a variation in their molar mass. Deviations from the E–D model $c_p(T) = N\ T + P\ T^3$ can be attributed to minimal free electrons within the sample matrix (Rao and Rao 1970; McSween 1987; Zolensky et al. 1997) and a multiplication of phonon vibrational modes due to crystalline dislocations, inhomogeneity, porosity, and grain boundaries in the sample (Matsui and Osako 1979).

Using the specific heat capacity data ($2 < T < 300$ K), the Debye temperatures, Θ_D, for the five meteorites were calculated using a nonlinear numerical evaluation of the Debye integral for solids (Kittel 1996; Macke et al. 2019) and those values are indicated in Table 1. In addition to Θ_D, the effective molar mass was calculated using a similar integral, allowing the effective molar mass as a free parameter and fitting to the experimental data. It is noted that both Θ_D and the effective molar mass calculated values are similar across this group of samples, which should be expected given this class of meteorites.

Thermal Expansion

Thermal expansion is the tendency of matter to change its shape in response to a change in temperature. As temperature increases, the average atomic kinetic energy of material rises. When the kinetic energy rises, the atoms oscillate with anharmonic potentials in greater amplitudes about their fixed points and the material expands to maintain a greater average separation between atoms (Levy 1968); this is in contrast to harmonic potentials that do not contribute to thermal expansion. Considering thermal expansion in one dimension, the magnitude of this effect is measured by the coefficient of linear expansion, α_L. This coefficient is defined as the fractional change in length, ΔL per unit change in temperature, ΔT and the equation $\Delta L = \alpha_L\, L_O\, \Delta T$ relates this phenomenon to the initial length L_O. For most isotropic crystals, the temperature dependence of α_L is proportional to c_p and has a T^3 dependence as $T \rightarrow 0$ K. At temperatures well beyond the Debye temperature, θ_D, the coefficient of linear expansion is constant (Aschroft and Mermin 1976).

Materials that contract with increasing temperature are said to experience negative thermal expansion (NTE); such materials are somewhat rare and this effect usually occurs within a limited temperature range. Often non-monotonic NTE behaviors occur with increasing temperature resulting from lattice strain, magnetic transitions (Takenaka and Takagi 2005), or crystallographic phase changes in the material (Evans and Mary 2000; Arvanitidis et al. 2003). However, there are materials, particularly zeolites (Marinkovic et al. 2004) or other compounds such as faujasite (Attfield and Sleight 1998b), where a type of NTE (Grima et al. 2006; Miller et al. 2009) appears due to the bridging molecules between layers. These thermally driven bond length modifications of bridge molecules can appear in bulk samples as NTE (Attfield and Sleight 1998a).

The thermal expansion of the CM2 samples was measured from 5 to 300 K and the expansion coefficients, α_L as a function of temperature, are shown in Fig. 5. From the lowest temperatures until about 200 K, we observe monotonic α_L behavior consistent with a composite solid material, which is roughly proportional to c_p. In between 200 and 240 K, all the samples exhibit large NTE features whose minima occur at about 235 K. As temperature increases, the NTE is followed by a sudden expansion, where the α_L of only one sample (NWA 7309) recovers to a level slightly higher than prior to the NTE onset.

The depth of the transition and minima varies somewhat from sample to sample, but the onset T is consistent across the different CM2 samples. From this, we conclude that the mechanism of the NTE is dependent on the common structure and origin of the material. Some ordinary chondrites—Cronstad (H5), NWA 11344 (L3-4), NWA 11038 (L3), as well as lunar meteorites (NWA 8687, NWA 6950)—were measured under the same experimental conditions with no evidence of such a transition. The data of Fig. 5 were

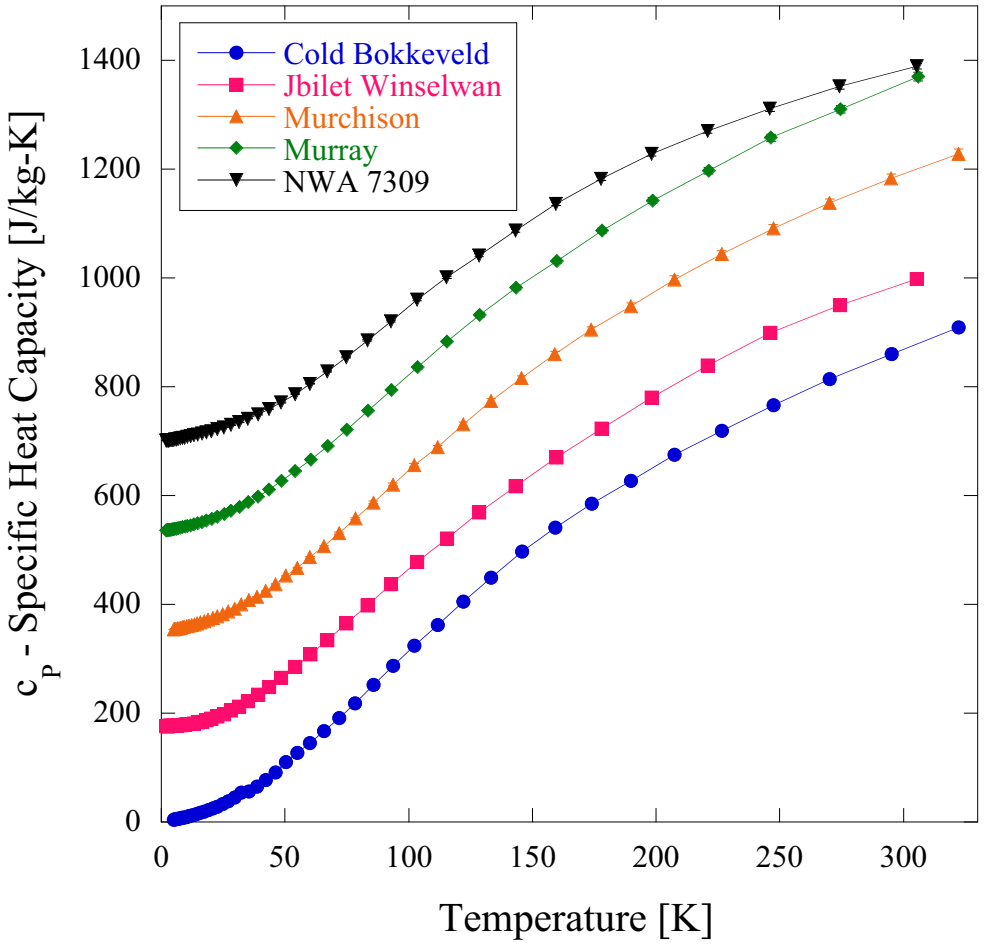

Fig. 4. Specific heat capacity (c_p) versus temperature was measured using a thermal relaxation technique for samples of ~20 mg and approximate dimensions of ~1 × 3 × 3 mm. The data are offset on the vertical axis by multiples of +175 J kg^{-1} K^{-1} for clarity. Lines are added as a guide to the eye. Error bars are present but smaller than the data symbols. (Color figure can be viewed at wileyonlinelibrary.com.)

Table 3. For the specific heat capacity versus temperature data shown in Fig. 4, coefficients G, H, J, L, and M were calculated, as a fit to the polynomial formula: $c_p(T) = G + H\ T + J\ T^2 + L\ T^3 + M\ T^4$ for $2 \le T \le 300$ K. Coefficients N and P for the low-temperature specific heat capacity data for $2 < T < 25$ K were fit to the equation, $c_p(T) = N\ T + P\ T^3$. In this function, the first-order term ($N\ T$) represents the low-temperature electronic portion of c_p and the cubic term ($P\ T^3$) indicates the lattice contribution according to Debye theory.

Meteorite	G × 10^{-1} (J kg^{-1} K^{-1})	H × 10^{-2} (J kg^{-1} K^{-2})	J × 10^{-2} (J kg^{-1} K^{-3})	L × 10^{-4} (J kg^{-1} K^{-4})	M × 10^{-7} (J kg^{-1} K^{-5})	N × 10^{-1} (J kg^{-1} K^{-2})	P × 10^{-4} (J kg^{-1} K^{-4})
Cold	2.168	42.581	4.425	−2.060	2.853	8.616	7.504
Bokkeveld Jbilet	−8.950	33.847	4.162	−1.927	2.686	3.498	9.106
Winselwan Murchison	−7.507	56.401	3.831	−1.726	2.319	8.865	6.864
Murray	4.394	33.636	4.123	−1.913	2.688	7.516	8.168
NWA 7309	23.901	−6.342	4.071	−1.867	2.561	6.239	7.039

taken while cooling the sample; data taken during sample warming show similar curves, with a hysteresis of about 20 K, shifting the average transition temperature to 255 K. Such hysteretic effects are common in materials when the retardation of the internal forces and friction acting upon a material is

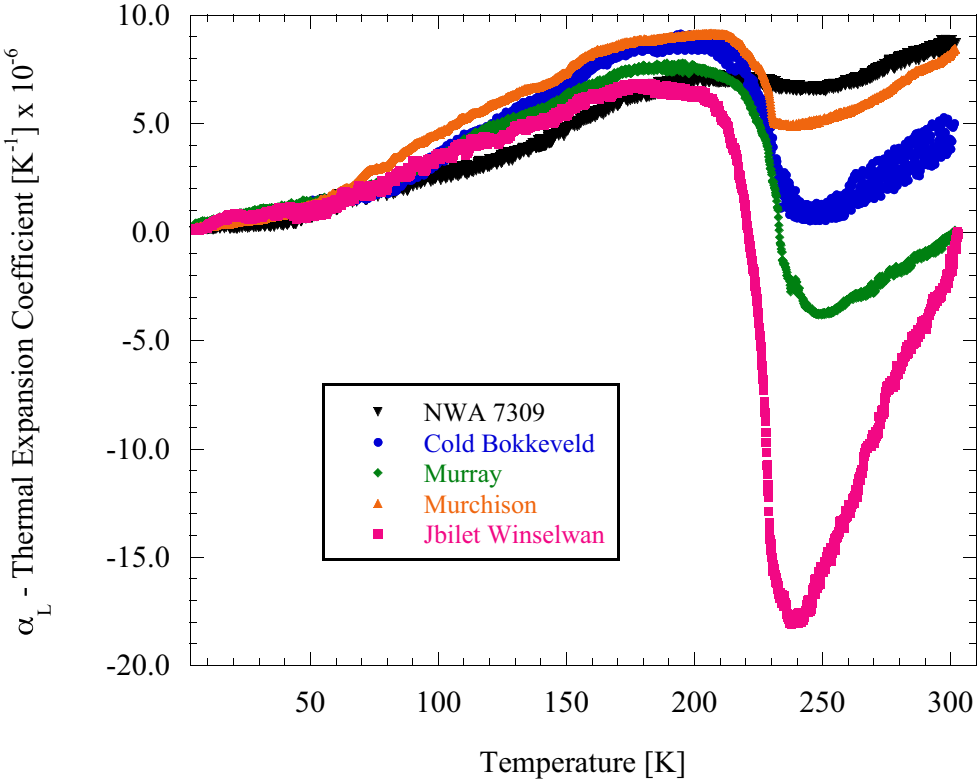

Fig. 5. Linear thermal expansion (α_L) versus T measurements indicate NTE across a broad T range which occurs for different samples at approximately the same temperature ~235 ± 1 K. Measurements shown were taken at a cooling rate of 0.25 K min^{-1} on a capacitive dilatometer with a resolution of ~0.8 Å (~8×10^{-11} m). Error bars are included and are smaller than the symbols. (Color figure can be viewed at wileyonlinelibrary.com.)

changed by a reduction or increase of thermal energy (Moore and Geyer 1974; Zhang et al. 2014).

The unusual NTE behavior observed at ~235 K is likely due to the contraction of the layered structure of the phyllosilicates that dominate the mineralogy of the CM2 meteorites. Many studies on CM2 meteorites show that aqueous alteration reactions of anhydrous precursor materials convert them to hydrous phyllosilicates, and trap volatiles in their crystal structure in the chemical form of H^+ and (hydroxyl) OH^- ions, as described by Howard et al. (2009). Similarly, infrared spectroscopy has been used by Beck et al. (2010) on Orgueil (CI) and Boriskino (CM2) meteorites to probe the OH and H_2O group vibrational behavior above 300 K.

The phyllosilicates in the CM2 meteorites are dominated by serpentine group minerals with a representative formula $(Al, Mg, Fe)_3Si_2O_5(OH)_4$ (McAdam et al. 2015). Thus, serpentinized minerals are layered silicate compounds with a stacked pattern of tetrahedral and octahedral sheets, which are strongly bonded together to form multiple parallel layers. Sheets of interconnected six-member rings of SiO_4^{-4} tetrahedra extend outward in infinite sheets. Three of the four oxygens from each tetrahedron are shared with other tetrahedra. The oxygens at the fourth corner of the tetrahedron form part of an immediately adjacent octahedral sheet and are linked by shared OH groups. The aqueous formation environment of the CM2 meteorites provides the phyllosilicates abundant hydroxyl ions (OH^-), which are located at the center of the six-membered rings. With the additional hydroxyl group, the basic building block between the layers becomes $Si_2O_5(OH)^{-3}$. Chemically abundant cations in the CM2 matrix such as Fe^{2+}, Al^{2+}, and Mg^{2+} bond to the $(OH)^-$ in an octahedral coordination (Bailey 1980; Brown 1984; Beck et al. 2010). Thus, these octahedral groups form a continuous layer and chemically bond with the tetrahedral sheets to form stable planes (Bish 1993; Burns 1993; Drits et al. 1993; Beaufort et al. 1998; Howard et al. 2009; Che et al. 2011). In order to visualize the parallel tetrahedral and octahedral sheets with the oxygen and hydroxyl (in projection) groups linked to upper and lower cations, Fig. 6 is shown (Bailey 1980; Brown 1984). This cross section of tetrahedral and octahedral sheets (1:1) is typical for phyllosilicates derived from serpentine or kaolin type clay.

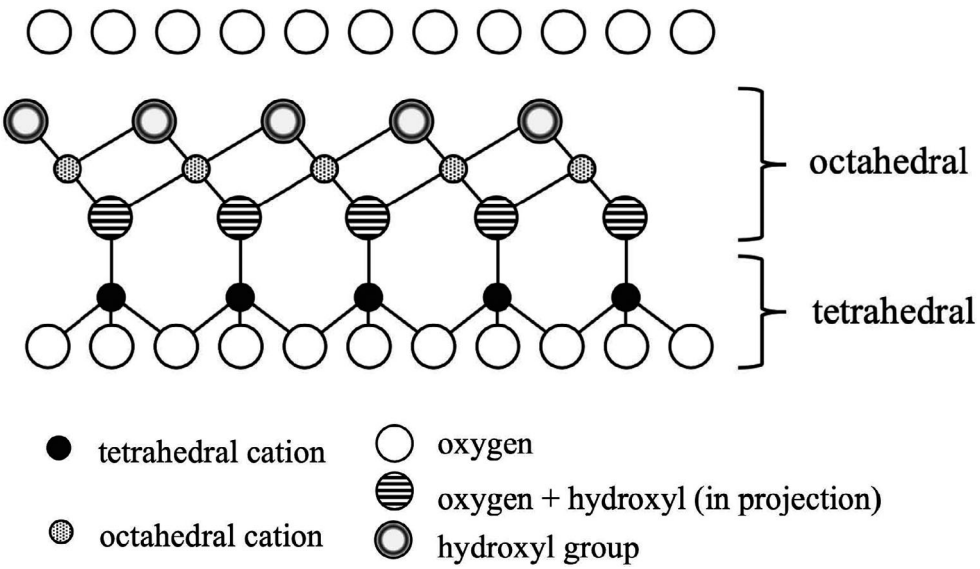

Fig. 6. This is a cross-sectional view of tetrahedral and octahedral sheets (1:1) linked by oxygen and hydroxyl (in projection) for a phyllosilicate material representing serpentine or kaolin type clay (Bailey 1980; Brown 1984).

In order for a material to display NTE, there must be a structural phenomenon that outweighs the usual tendency of bonds to expand with increasing temperature (Evans 1999). To understand the thermal expansion of complex inorganic materials such as CM2 meteorites, one must consider the population of all vibrational modes at a given temperature (Barron 1957). Phonons are quantized modes of vibration and possess a range of different frequencies, wavelengths, amplitudes, and phases (Miller et al. 2009). We consider here the phonon vibrational modes of the bridging molecules (M–O–M bonds) between tetrahedral and octahedral silicate layers, where the behavior of the longitudinal and transverse components is independent and can be activated at different temperatures (Blackman 1957). Here, the first "M" is identified with a tetrahedral cation (e.g., Fe^{2+}, Al^{2+}, Mg^{2+}), which is bonded to "O" (oxygen) that is in turn bonded to the second "M" identified as an octahedral cation (Bailey 1980; Brown 1984).

To illustrate this vibrational phenomenon, a "guitar string" analogy (Evans 1999; Miller et al. 2009) is depicted in Fig. 7. Longitudinal modes (along the M–O–M bond) tend to increase interatomic M–M distances, whereas in transverse vibrational modes, the M–O distance remains unchanged, but the M–M distance will decrease. It is assumed that transverse modes have lower excitation energy at very low temperatures ($T < 150$ K), but as the temperature rises to the onset of the NTE ($T \sim 200$ K), the transverse modes begin to dominate over the longitudinal modes. Therefore, the thermal expansion response of a material (negative or positive) will depend on whether the longitudinal or transverse modes dominate at a particular temperature. Thus, the layered tetragonal/octahedral silicate structure, common to the CM2 meteorites, allows the dominance of the transverse vibratory-type motion of the interlayer bonds and produces a broad NTE behavior centered at ~235 K. It is likely that this phenomenon is universal for CM2 meteorites simply due to their composition, derived from a formation of the serpentine group minerals. It is also likely to be found in any meteorite group that is rich in serpentine group minerals, such as CI (Ivuna-like), CM (Mighei-like), and CR (Renazzo-like) carbonaceous chondrites due to the abundance of water and phyllosilicate formation (Velbel et al. 2012).

According to the thermodynamics of the Debye model and the Ehrenfest relation for second-order phase transitions, α_L is proportional to c_p (Aschroft and Mermin 1976); thus, evidence of any significant NTE should be accompanied by a simultaneous fluctuation in specific heat (Jaeger 1998; Takenaka 2012; Moin 2013). In order to confirm any fluctuation in specific heat, the CM2 samples were remeasured from 190 to 280 K at 1 K intervals. These c_p versus T data (open symbols) are shown in Fig. 8 along with its temperature derivative, dc_p/dT versus T (solid symbols). There is a slight change in slope for c_p versus T for all CM2 samples in the vicinity of 235 K, which is revealed by its temperature derivative as a broad transition. These transitions are consistent with the temperature-dependent transitions of thermal expansion reported in Fig. 5. Due to the proportionality between linear

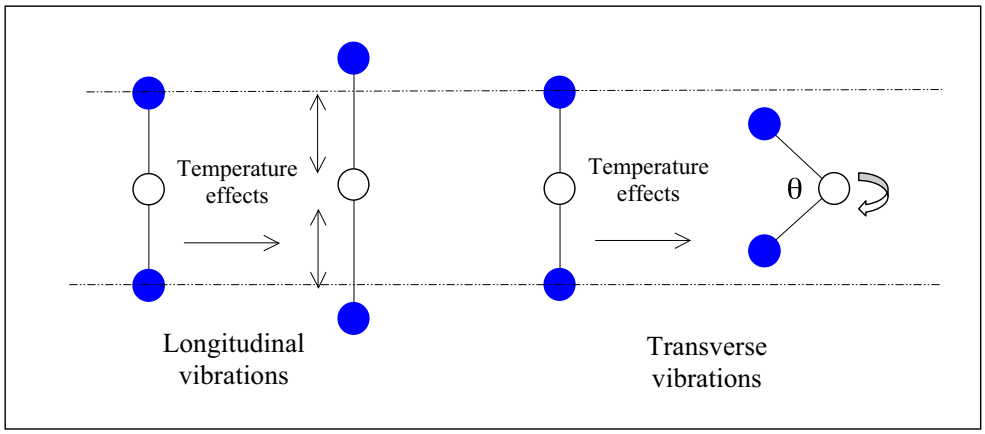

Fig. 7. The "guitar string" (Evans 1999; Miller et al. 2009) bonding schematic shows longitudinal mode vibrations (left) of M–O–M chemical bonding (M—cation [blue], O—oxygen [no color]) found between tetrahedral and octahedral layered silicate structures. Transverse vibrations (right) allow $\theta < 180°$ and are responsible for NTE as transverse mode vibrations dominate longitudinal vibrations. (Color figure can be viewed at wileyonlinelibrary.com.)

thermal expansion and specific heat, one might anticipate a significant change in specific heat at ~235 K given the large NTE shown by CM2 meteorites. Since the Debye model assumes that sample materials are dense, highly ordered crystalline solids, the relatively small fluctuations in c_p versus T are likely a consequence of the porosity (15.0–26.4%) and low symmetry of the CM2 meteorites (Kirchner 1964; Consolmagno et al. 2008; Howard et al. 2009).

Thermal Diffusivity and Thermal Inertia

Heat transfer in asteroids and meteors is directly related to their formation and ongoing evolution. Understanding the temperature-dependent behavior of heat energy in these materials gives insight into their evolutionary process and their thermal constraints.

In order to trace the thermal evolutionary process of meteoritic materials, we have calculated the thermal diffusivity of sample CM2 meteorites from 5 to 300 K. Thermal diffusivity (D_T) is a material-specific property characterizing the time-dependent heat conduction through a body. Its value describes the rate a material or a cross section through it reacts to changes in temperature. Thermal diffusivity has units of area per time ($m^2\ s^{-1}$) and is calculated by the formula, $D_T = \kappa\ \rho^{-1}\ c_p{}^{-1}$ where κ is thermal conductivity, ρ is mass density, and c_p is specific heat capacity at a constant pressure (Kittel and Kroemer 1980).

To calculate values of thermal diffusivity, the temperature-dependent κ and c_p data displayed in Figs. 3 and 4 were linearly interpolated to create a plot of D_T versus T shown in Fig. 9. Sample densities are shown in Table 1 and were considered as virtually constant across the temperature range. The data are plotted on a log (T) format to emphasize the relatively constant response of D_T in these meteorites for $T > 100$ K where $D_T \sim 1 \times 10^{-6}\ m^2\ s^{-1}$ as well as the significant rise in D_T to a maximum at low temperature. For $T < 100$ K, D_T rises in all samples with the exception of NWA 7309 to a broad maximum between 5 to 12 K before decreasing to a zero value at $T = 0$ K. Since D_T is proportional to κ, the curve for NWA 7309 in Fig. 9 is expected to decrease rapidly toward zero at a temperature below 2 K, which is below the experimental temperature range of our cryogenic refrigerator. It can be argued that for temperatures of $300 < T < 400$ K, the D_T behavior should remain constant due to a saturation of κ and c_p. However, due to the high water (10–15%) and hydroxyl content in CM2 samples, the value of D_T is likely to change significantly for $T > 400$ K as these components are expelled from the matrix by vaporization. Similar observations of a decrease in D_T with increasing temperature, followed by a relatively constant value of D_T at 200–300 K, were made by Vosteen and Schellschmidt (2003) and Whittington et al. (2009) on terrestrial samples and by Matsui and Osako (1979) on a series of Yamato meteorites.

In order to obtain comparative values of thermal diffusivity for all samples, the empirical formula $D_T(T) = R + S\ T^{-1} + U\ T^{-2} + V\ T^{-3} + W\ T^{-4}$, following the analysis of Pertermann and Hofmeister (2006), was used to analyze the data for $T > 10$ K. The constants R, S, U, V, and W are obtained by the least-squares fit and are listed in Table 4.

Thermal inertia (Γ) is a quantity related to thermal diffusivity and represents the ability of a material to conduct, store, and reradiate heat during its diurnal–nocturnal cycle (Delbó et al. 2015). Thermal inertia is calculated by the formula $\Gamma = (\kappa\ \rho\ c_p)^{1/2}$ with

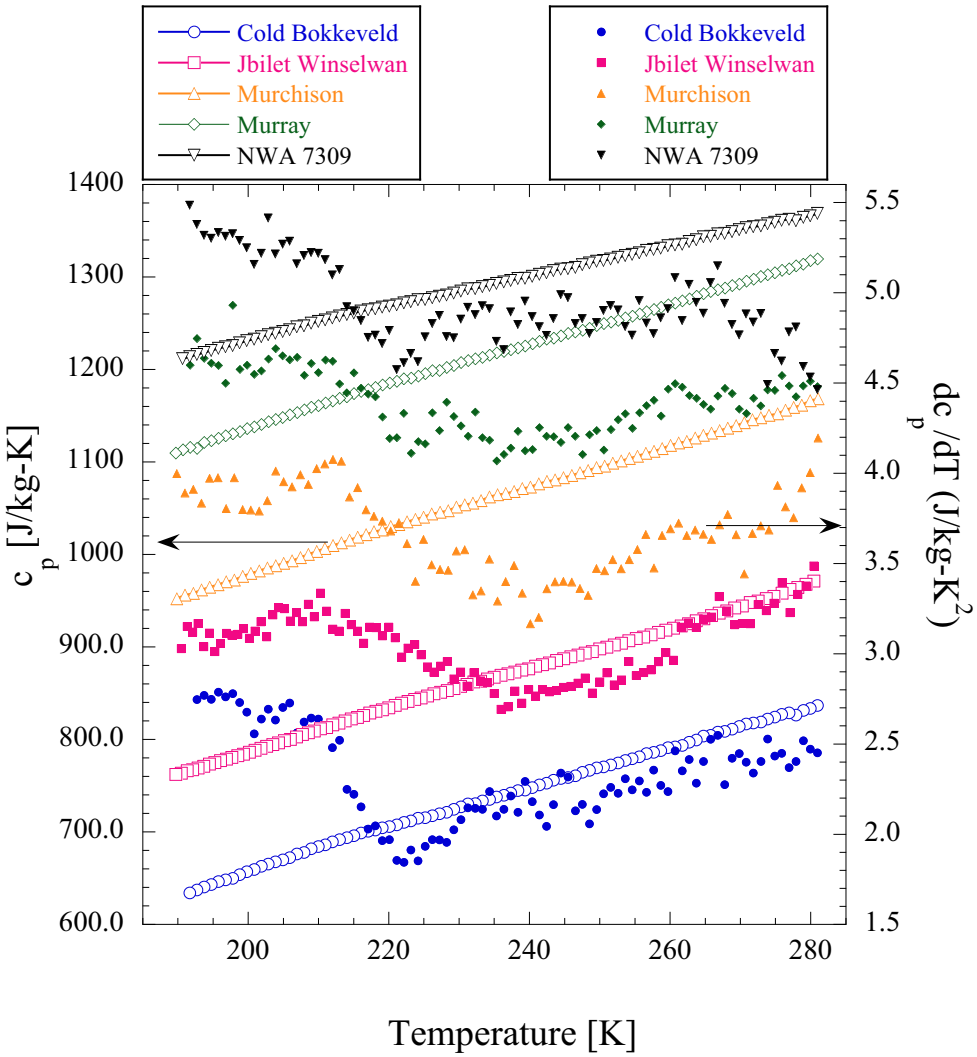

Fig. 8. Specific heat capacity (c_p) versus T (open symbols) are plotted along with dc_p/dT versus T (solid symbols) for all samples in the temperature range 190–280 K. The data for both c_p and dc_p/dT are offset in the vertical scale for clarity. The c_p versus T data reveal in its derivative dc_p/dT a broad thermodynamic transition in a temperature region similar to that shown by linear thermal expansion; see Fig. 5. (Color figure can be viewed at wileyonlinelibrary.com.)

SI units of J m^{-2} K^{-1} s$^{-½}$. In the context of planetary science, while surface mineralogy and rock strata will have a direct effect on a typical terrestrial planetary surface, Γ depends predominantly on the physical properties of the near surface materials such as particle grain size, hardness, average density, porosity, rock abundance, and the exposure of bedrock (Jakosky 1986).

The change from compact rock to loose regolith will greatly affect the value of the thermal inertia. The most dominant effect of regolith growth on thermal inertia is the decrease in thermal conductivity due to a reduction in the phonon conduction of heat energy through granular material. This change in conductivity is not linearly proportional to degree of macroporosity in the regolith; a surface that is 50–70% porous can have a thermal conductivity that is orders of magnitude lower than that of a compact rock of the same material. (Sakatani et al. [2017] have measured this effect for spherical glass beads of constant radius. While one cannot apply their specific results directly to the far more complex geometry of multimineralic regoliths, the general principle remains that thermal conductivity in a highly porous material can be reduced by several orders of magnitude.)

The density of the regolith is, by definition, linearly proportional to its porosity; thus, while the regolith's change of density does have an effect on the thermal inertia, it is much less than the effect of the changing thermal conductivity.

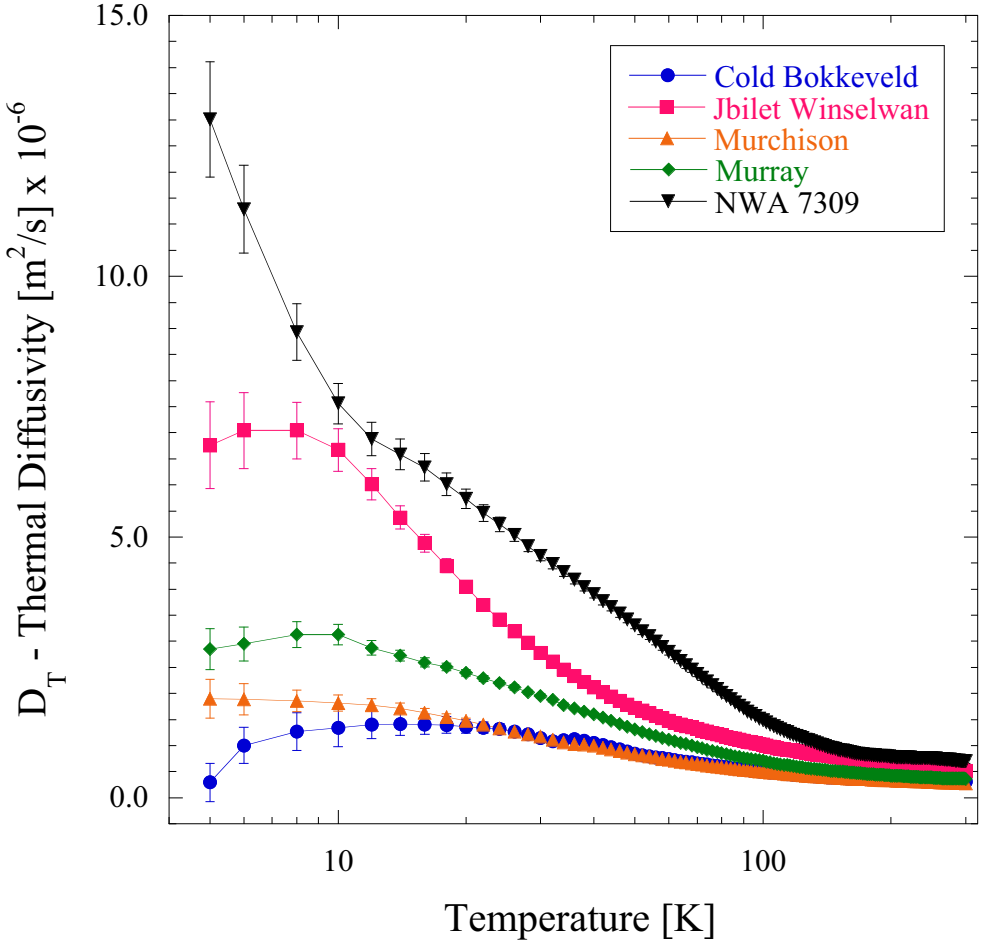

Fig. 9. The calculated values for thermal diffusivity (D_T) versus temperature values for the CM2 meteorite samples are shown here. Data show little variation for $T \geq 100$ K but exhibit a significant increase at $T < 100$ K. These data are consistent with our previous D_T measurements on ordinary (H, L) and carbonaceous (CV3) chondrites across the same temperature range. Lines are added as a guide to the eye. (Color figure can be viewed at wileyonlinelibrary.com.)

The heat capacity depends only on the vibrational states of the various minerals present. For a given material, this is not at all affected by the macroscopic physical state of the minerals, so long as the processes that produce a regolith do not materially change the mineralogy of the material.

That said, once an asteroid's surface has been converted into a regolith, heat capacity is the only factor in its thermal inertia that will significantly change with temperature above 100 K. For temperatures lower than 100 K, both heat capacity and thermal conductivity will be strong functions of temperature, both dropping as the temperature drops.

One important reason to study thermal inertia is that it is a determining factor in the temperature distribution over the surface of interplanetary bodies, which governs the magnitude of the Yarkovsky and YORP effects (Čapek and Vokrouhlický 2004; Bottke et al. 2006; Delbó et al. 2007; Vokrouhlický et al. 2015). These effects influence the rate and orientation of an asteroid's spin, and the slow movement of small asteroids and meteoroids from their place of formation to other regions of the solar system and the possible gravitational effects of a near-Earth approach (Bottke et al. 2002). The majority of thermal inertia studies of asteroids and moons entail spectroscopic measurements (Harris and Davies 1999; Müller et al. 2004; Putzig et al. 2005) using remote observational techniques, which produce models of asteroidal behavior (Lagerros 1996). The purpose of our investigation into thermal inertia here is to examine the temperature dependence of Γ on CM2 samples that at some point in their history were part of an asteroid or parent body surface.

Temperature-dependent thermal inertia calculations for the CM2 samples are shown in Fig. 10. The Γ data are calculated by interpolating thermal conductivity and specific heat capacity data shown in Figs. 3 and 4 with the bulk density as noted in Table 1. Density is assumed

Table 4. Coefficients R, S, U, V, and W were calculated for the empirical equation $D_T(T) = R + S\ T^{-1} + U\ T^{-2} + V\ T^{-3} + W\ T^{-4}$ (Pertermann and Hofmeister 2006). Calculations for thermal diffusivity as a function of absolute temperature include data (see Fig. 9) for $T > 10$ K.

Meteorite	R × 10^{-7} (m^2 s^{-1})	S × 10^{-5} (m^2K s^{-1})	U × 10^{-4} (m^2K^2 s^{-1})	V × 10^{-2} (m^2K^3 s^{-1})	W (m^2K^4 s^{-1})
Cold	2.006	2.624	6.464	−2.053	0.133
Bokkeveld Jbilet	3.005	6.805	2.599	−0.186	−0.015
Winselwan Murchison	1.649	3.450	0.173	−0.546	0.037
Murray	1.809	4.561	10.229	−3.048	0.196
NWA 7309	1.189	12.915	24.192	−8.141	0.549

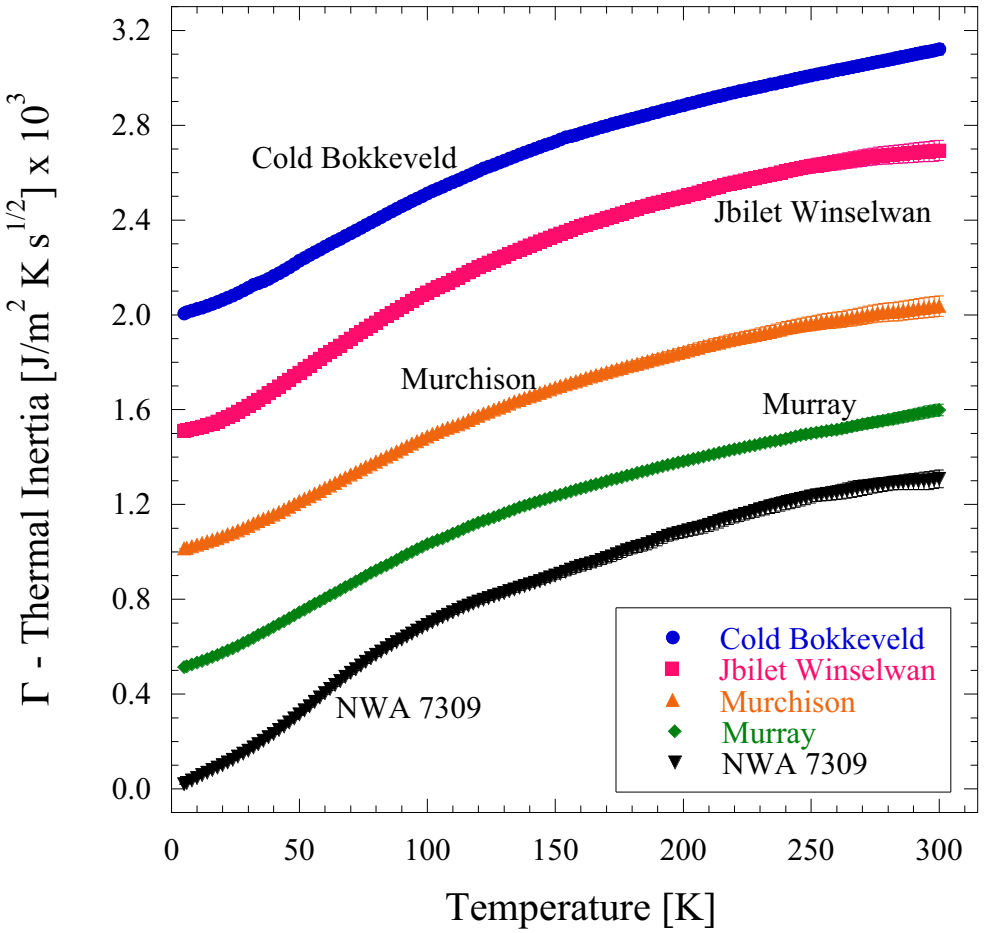

Fig. 10. Calculated thermal inertia (Γ) versus temperature values for the CM2 meteorite samples are shown. Data are offset by multiples of +0.5 x 10^3 J m^{-2} K^{-1} $s^{-1/2}$ on the vertical axis for clarity. Each curve shows an inflection point in the curve at 55–60 K. Error bars are present but are often smaller than the data symbols except at high T. (Color figure can be viewed at wileyonlinelibrary.com.)

to be constant across this experimental temperature range due to a very small effective volume contraction shown in Fig. 5. The Γ data show a strong temperature dependence with two distinct regimes as it increases from the lowest temperatures at 10 to ~10^3 J m^{-2} K^{-1} $s^{-½}$ at 300 K. Each curve in Fig. 10 indicates an inflection point or particular change of slope as the temperature rises to about 55–60 K. Above 60 K, the pace of this rise diminishes, and a gradual saturation occurs as temperatures approach 300 K. This change in curvature in Γ at ~55 to 60 K is confirmed by plotting $d\Gamma/dT$ with respect to temperature (Fig. 11). Such an inflection point in the data is a consequence of the change in magnitude of c_p, around 55–60 K, which is an essential factor of

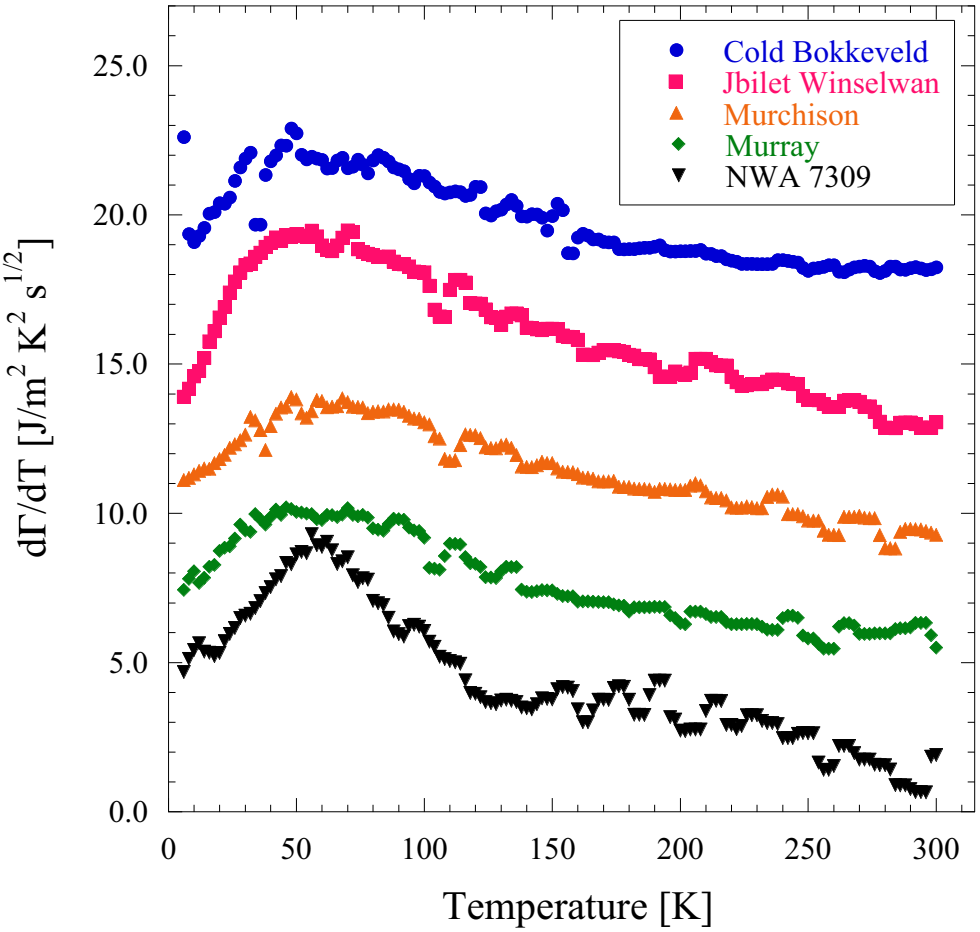

Fig. 11. The derivative of thermal inertia (dΓ/dT) versus temperature illustrates a change of curvature in Γ at ~55 to 60 K. Data are offset by multiples of +4 J m^{-2}K^{-2} s$^{-1/2}$ on the vertical axis for clarity. (Color figure can be viewed at wileyonlinelibrary.com.)

thermal inertia, $\Gamma = (\kappa\ \rho\ c_p)^{1/2}$. Since mass density is considered a constant in our calculation and thermal conductivity changes linearly below 75 K (see Fig. 3), neither contribute significantly to the curve inflection at 55–60 K.

Is it possible, or likely, that temperatures of 55–60 K might be reached on the nighttime side of slowly rotating asteroids? The answer is not at all straightforward. The temperature at any point on an asteroid's surface is a function of its subsolar latitude, and this depends on how quickly an asteroid surface in sunlight warms up, how quickly the night side cools off, and how quickly the asteroid rotates. The rate of heating and cooling is, of course, directly dependent on the thermal inertia, which is in turn dependent on the temperature of the material. However, in addition, the YORP effect noted above, which is dependent on the thermal inertia, also alters the spin rate of the asteroid. Thus, to model the actual temperatures, inertias, and spin rates of a given asteroid requires a highly nonlinear model beyond the scope of this paper.

DISCUSSION

Physics of Thermal Expansion

The thermal expansion data shown for the CM meteorites are the first reported observation of NTE data derived from extraterrestrial samples. The common behavior shown in these samples with a transition at T ~ 235 K is a likely indicator of a behavior present in all CM2 meteorites. These results imply that the thermal expansion technique can be used to provide insight into the physical behavior of meteorites that contain similar mineralogies. Similar experimental data can be shown for more recent CM2 finds: NWA 10827, NWA 10126, Aguas Zarcas, NWA 12778, and NWA 8534 (CM1/2) in a paper in preparation.

Implications for Modeling and Asteroid Orbital Evolution

These data provide fundamental experimental parameters for a range of planetary science issues including ISRU, regolith formation, the strength of asteroidal materials, and asteroidal responses to the Yarkovsky and YORP effects. The broad NTE behavior in CMs centered an ~235 K is an important factor in the evolution of CM mineralogy asteroids within their physical environment in the inner solar system.

The expansion, contraction, and expansion again in a narrow temperature range around 235 K likely induce much stronger stress on surrounding materials in what is essentially a conglomerate of dissimilar materials. The issue is not only the change of sign of the volume change but also the large degree of volume change over a very short temperature interval. The implication is that phyllosilicate-rich asteroid parent bodies, where stresses can occur as the phyllosilicate expansion or contraction behavior contrasts with the behavior of the other minerals present, or small temperature differences of neighboring materials within the body, may be more susceptible to physical weathering and disaggregation that meteorites of other mineralogies. If this is true, then phyllosilicate-rich asteroids, such as the parent asteroids of CI, C2, CM, and CR carbonaceous chondrites, should tend to weather physically much faster than other carbonaceous chondrites, depending on their content of serpentine group minerals. For instance, CR carbonaceous chondrites have varying amounts of serpentine ranging from 20 to 70 wt%. The magnitude of this variation would probably drive the rate of physical weathering in CR parent bodies.

The bottom line for any volatile-rich carbonaceous chondrite is that this NTE behavior would lead to faster breakup of coherent materials on the asteroid surface. The surface boulders on volatile-rich asteroids sunward of the main asteroid belt would have weaker surface layers than anhydrous carbonaceous chondrite or ordinary chondrite parent bodies. This increased relative stress in the inner solar system may also lead to a more rapid breakup of phyllosilicate-rich asteroid parent bodies in the NEO population. Such rapid breakup is suggested for primitive carbonaceous meteorites/asteroids by Granvik et al. (2016) for low albedo NEAs where they are preferentially destroyed at small perihelion distances. Such observations by Granvik may find their origin in the NTE centered at 235 K described our present work. In contrast, volatile-rich asteroid parent bodies in more distant and colder solar system regions such as the main asteroid belt, the Trojans, and the Kuiper belt—which have never experienced temperatures warm enough to activate the NTE excursions—would not exhibit increased physical degradation and weaker surface materials. The NTE excursions are significant factors in the physical evolution of volatile-rich asteroids and must be taken into consideration in designing exploration missions and ISRU technology that interacts with the surface material of these bodies.

These data and our previous work (Opeil et al. 2010, 2012) also show that mineralogy matters in the thermal response of asteroids. Specific heat capacity, thermal conductivity, thermal diffusivity, thermal inertia, as well as thermal expansion are strong functions of mineralogy and temperature. Many modeling efforts, including modeling of the Yarkovsky and YORP effects, typically treat these data as a constant across all asteroid types (Bottke et al. 2002; Vokrouhlický et al. 2015). Opeil et al. (2010) showed that thermal conductivity for the major meteorite groups varies by at least a factor of 10 over the temperature range of 2–350 K. The response of an enstatite chondrite parent body will be very different than the response of a volatile-rich carbonaceous chondrite parent body. It is useful to also remember that these meteorites are essentially conglomerates of sometimes very dissimilar minerals. As a result, their response is going to be quite different from the thermal properties of the original pure minerals.

The dependence of thermal diffusivity with temperature as illustrated in Fig. 9 will have important consequences for our understanding of the early thermal evolution of small bodies in the outer solar system. Outer solar system moons are a mixture of rocky and icy components, and the thermal properties of CM2 meteorites may be a reasonable analog for the thermal properties of the rocky component. Strictly speaking, our conclusions about the temperature dependence of thermal diffusivity and thermal inertia apply only to the CM2 material measured here. However, our measurements are in agreement with the more general theory of the variation of conductivity and heat capacity with temperature at low temperatures, as described above, and thus ought to be generally true for all materials, including ices.

In Fig. 9, one sees that the diffusivity at very low temperatures is significantly higher than that measured at room temperature. Recall that diffusivity depends on the ratio of conductivity to heat capacity; while the conductivity drops with temperature, as reported earlier, the heat capacity also drops with temperature. As a result, the diffusivity stays relatively constant down to about 200 K. But below that temperature, the drop in heat capacity dominates over that in conductivity, resulting in a net increase in thermal diffusivity.

The characteristic time for thermal diffusion varies inversely with diffusivity; thus, as diffusivity increases,

the characteristic time decreases. We conclude that small bodies should heat up faster than previous models had predicted. As temperatures drop from 200 to 100 K, relevant to the Jovian moons, the thermal diffusivity of the rocky material may increase by as much as a factor of two; the characteristic heat diffusion time for a Jovian moon or a Trojan asteroid could be only half that which might be calculated on the basis of room temperature data for pure minerals. And at temperatures below 100 K, characteristic of the moons of Saturn, Uranus, and Neptune or of centaurs, KBOs, and outer dwarf planets, the effect should be more dramatic—by perhaps as much as a factor of five.

The case of thermal inertia is far more dramatic, as seen in Fig. 10, because it depends on the product of conductivity and heat capacity (to the ½ power). From 200 K down to 20 K, we see that the thermal inertia drops by an order of magnitude. While it is true that the thermal inertia of larger bodies (>10 to 100 km diameter) is dominated by surface porosity, if smaller asteroids do not have significant regoliths, then the thermal inertia of asteroids smaller than a few km may not be all that different from that of the presumptive material from which the asteroid is made. This suggests that smaller and colder outer solar system bodies will be less strongly affected by Yarkovsky and YORP effects than previously assumed. There is also an interesting nonlinearity here; the lower the thermal inertia, the colder the nighttime surface, which in turn drives the thermal inertia even lower.

Another factor to remember is that the temperature dependence of thermal properties is far from linear. Take, for example, the rate of change of thermal inertia for CM2 carbonaceous chondrites shown in Fig. 11. By far the largest change and thermal inertia comes in the temperature range centered around 55–60 K. This may be an important factor in how small asteroids respond to the Yarkovsky and YORP effects depending on their position in the asteroid belt. For the parent bodies of CM2 carbonaceous chondrites, their original position in the asteroid belt may drive how rapidly they can respond to Yarkovsky and YORP perturbations. This could result in some resonant exits from the asteroid belt being preferred to others simply on the basis of the thermal response of the surface material.

CONCLUSIONS

The data developed in this work have a number of implications for our view of the evolution and modeling of CM carbonaceous parent bodies.

- The thermal properties of CM carbonaceous chondrites (and all other meteorite types) are a strong function of temperature and mineralogy. The change in specific heat capacity, thermal conductivity, thermal diffusivity, and thermal inertia over our measured temperature range can be a factor of two or more. The change in heat capacity is seen across all temperatures measured; that in thermal conductivity is most evident below 100 K, as is the change in inertia and diffusivity which both rely on conductivity.
- The rate of change in thermal parameters is often not linear over the temperature range measured. The fastest rate of change may be concentrated in dynamically important temperature ranges and impose a strong selection effect on dynamic effects like Yarkovsky and YORP perturbations. This could result in some resonant exits from the asteroid belt being preferred to others simply on the basis of the thermal response of the surface material.
- Mineralogy matters in the thermal properties of meteorites and their parent asteroids. Varying mineralogy across asteroid parent bodies does mean that one assumed number is unlikely to replicate thermal parameters for all asteroids.
- The broad NTE behavior in CMs centered at ~235 K produced by serpentine group phyllosilicates is likely an important factor in the evolution of serpentine-rich mineralogy asteroids in response to the physical environment of the inner solar system. Serpentine-rich NEO parent bodies are likely to be subjected to stronger physical weathering, degradation of surface strength properties, and increased dust production. This increased relative stress in the inner solar system may also lead to a more rapid breakup of phyllosilicate-rich asteroid parent bodies in the NEO population.

Fundamentally, the thermal properties of the parent asteroids are going to vary, and sometimes vary substantially, with temperature and mineralogy.

Acknowledgments—This work is supported by NASA, the Solar System Exploration Research Virtual Institute (SSERVI), and the Center for Lunar and Asteroid Surface Science (CLASS) under NASA Cooperative Agreements NNA14AB05 and 80NSSC19M0214. The authors would like to thank M. Delbó, and an anonymous reviewer for their reviews which substantially improved the quality of this manuscript, and Scott Sandford for his excellent facilitating of the review process as the associate editor. We wish to thank G. Schmiedesoff for assistance with the dilatometry analysis.

Editorial Handling—Dr. Scott Sandford

REFERENCES

Arvanitidis J., Papagelis K., Margadonna S., Prassides K., and Fitch A. N. 2003. Temperature-induced valence transition and associated lattice collapse in samarium fulleride. *Nature* 425:599–602.

Aschroft N. W. and Mermin N. D. 1976. *Solid state physics*. New York: Harcourt College Publishers. 826 p.

Attfield M. P. and Sleight A. W. 1998a. Exceptional negative thermal expansion in AlPO4-17. *Chemistry of Materials* 10:2013–2019.

Attfield M. P. and Sleight A. W. 1998b. Strong negative thermal expansion in siliceous faujasite. *Chemical Communications* 1998-5:601–602.

Bailey S. W. 1980. Structures of layer silicates. In *Crystal structures of clay minerals and their X-ray identification*, edited by Brindley G. W. and Brown G. London: Mineralogical Society of Great Britain and Ireland. pp. 1–124.

Barron T. H. K. 1957. Gruneisen parameters for the equation of state of solids. *Annals of Physics* 1:77–90.

Beaufort D., Cassagnabere A., Petit S., Lanson B., Berger G., Lacharpagne J. C., and Johansen H. 1998. Kaolinite-to-dickit reaction in sandstone reservoirs. *Clay Minerals* 33:297–316.

Beck P., Quirico E., Montes-Hernandez G., Bonal L., Bollard J., Orthous-Daunay F.-R., Howard K. T., Schmitt B., Brissaud O., Deschamps F., Wunder B., and Guillot S. 2010. Hydrous mineralogy of CM and CI chondrites from infrared spectroscopy and their relationship with low albedo asteroids. *Geochimica et Cosmochimica Acta* 74:4881–4892.

Bish D. L. 1993. Rietveld refinement of the kaolinite structure at 1.5 K. *Clays and Clay Minerals* 41:738–744.

Blackman M. 1957. On the thermal expansion of solids. *Proceedings of the Physical Society* B70:827–832.

Bottke W. F. Jr, Vokrouhlický D., Rubincam D. P., and Broz M. 2002. The effect of Yarkovsky thermal forces on the dynamical evolution of asteroids and meteoroids. In *Asteroids III*, edited by Bottke W. F., Cellino A., Paolicchi P., and Binzel R. P. Tuscon, Arizona: University of Arizona Press. pp. 395–408.

Bottke W. F. Jr., Vokrouhlický D., Rubincam D. P., and Nesvorný D. 2006. The Yarkovsky and Yorp effects: Implications for asteroid dynamics. *Annual Review of Earth and Planetary Sciences* 34:157–191.

Brearley A. J. 2006. The action of water. In *Meteorites and the early solar system II*, edited by Lauretta D. S. and McSween H. T. Jr. Tuscon, Arizona: University of Arizona Press. pp. 587–624.

Britt D. T. and Consolmagno G. J. 2003. Stony meteorite porosities and densities: A review of the data through 2001. *Meteoritics & Planetary Science* 38:1161–1180.

Brown G. 1984. Crystal structures of clay minerals and related phyllosilicates. *Philosophical Transactions of the Royal Society of London Series A* 311:221–240.

Browning L. B., McSween H. T. Jr and Zolensky M. E. 1996. Correlated alteration effects in CM carbonaceous chondrites. *Geochimica et Cosmochimica Acta* 60:2621–2633.

Burns R. G. 1993. *Mineralogical applications of crystal field theory*, 2nd ed. Cambridge: Cambridge University Press. 551 p.

Čapek D. and Vokrouhlický D. 2004. The YORP effect with finite thermal conductivity. *Icarus* 172:526–536.

Cermak V. and Rybach L. 1982. Thermal properties: Thermal conductivity and specific heat of minerals and rocks. In *Landolt-Bernstein Zahlenwert and Funktionen aus Naturwissenschaften und Technik, Neue Serie, Physikalische Eigenschftender Gesteine*, edited by Angeneister G. Berlin, Germany: Springer Verlag. pp. 305–343.

Che C., Glotch T. D., Bish D. L., Michalski J. R., and Xu W. 2011. Spectroscopic study of the dehydration and/or dehydroxylation of phyllosilicate and zeolite minerals. *Journal of Geophysical Research* 116:E05007.

Consolmagno G. J., Britt D. T., and Macke R. J. 2008. The significance of meteorite density and porosity. *Chemie der Erde Geochemistry* 68:1–29.

Delbó M., dell'Oro A., Harris A. W., Mottola S., and Mueller M. 2007. Thermal inertia of near-Earth asteroids and implications for the magnitude of the Yarkovsky effect. *Icarus* 190:236–249.

Delbó M., Libourel G., Wilkerson J., Murdoch N., Michel P., Ramesh K. T., Ganino C., Verati C., and Marchi S. 2014. Thermal fatigue as the origin of regolith on small asteroids. *Nature* 508:233–236.

Delbó M., Mueller M., Emery J. P., Rozitis B., and Capria M. T. 2015. Asteroid thermophysical modeling. In *Asteroids IV*, edited by Michel P. Tucson, Arizona: University of Arizona Press. pp. 107–128.

Dilley N. R., Black R. C., Montes L., Wilson A., and Simmonds M. B. 2002. Commercial apparatus for measuring thermal transport properties range of 1.9-390 Kelvin. Proceedings, 2001 Material Research Society Symposium. Vol. 691, pp. G3.5.1–G3.5.6.

Drits V. A., Sakharov B. A., Salyn A. L., and Manceau A. 1993. Structural model for ferrihydrite. *Clay Minerals* 28:185–207.

El Mir C., Ramesh K. T., and Delbó M. 2019. The efficiency of thermal fatigue in regolith generation on small airless bodies. *Icarus* 333:356–370.

Evans J. S. O. 1999. Negative thermal expansion materials. *Journal of the Chemical Society, Dalton Transactions* 19:3317–3326.

Evans J. S. O. and Mary T. A. 2000. Structural phase transitions and negative thermal expansion in $Sc_2(MoO_4)_3$. *International Journal Inorganic Material* 2:143–151.

Fujii N. and Osako M. 1973. Thermal diffusivity of lunar rocks under atmospheric and vacuum conditions. *Earth and Planetary Science Letters* 18:65–71.

Granvik M., Morbidelli A., Jedicke R., Bolin B., Bottke W. F. Jr, Beshore E., Vokrouhlický D., Delbó M., and Michel P. 2016. Super-catastrophic disruption of asteroids at small perihelion distances. *Nature* 530:303–306.

Grima J. N., Zammit V., and Gatt R. 2006. Negative thermal expansion. *Xjenza* 11:17–29.

Grimvall G. 1999. *Thermophysical properties of materials*. Amsterdam, the Netherlands: Elsevier Science B. V. 422 p.

Haas J. L. Jr. and Fisher J. R. 1976. Simultaneous evaluation and correlation of thermodynamic data. *American Journal of Science* 276:525–545.

Harris A. W. and Davies J. K. 1999. Physical characteristics of near-earth asteroids from thermal infrared spectrophotometry. *Icarus* 142:464–475.

Hazeli K., El Mir C., Papanikolaou S., Delbó M., and Ramesh K. 2018. The origins of Asteroidal rock disaggregation: Interplay of thermal fatigue and microstructure. *Icarus* 304:172–182.

Hofmeister A. M., Branlund J. M., and Pertermann M. 2007. Properties of rocks and minerals—Thermal conductivity of

the Earth. In *Treatise on geophysics*, Volume 2. Amsterdam, the Netherlands: Elsevier Press. pp. 543–577.
Howard K. T., Benedix G. K., Bland P. A., and Cressey G. 2009. Modal mineralogy of CM2 chondrites by X-ray diffraction (PSD-XRD). Part 1: Total phyllosilicate abundance and the degree of aqueous alteration. *Geochimica et Cosmochimica Acta* 73:4576–4589.
Jaeger G. 1998. The Ehrenfest classification of phase transitions: Introduction and evolution. *Archive for History of Exact Sciences* 53:51–81.
Jakosky B. M. 1986. On the thermal properties of Martian fines. *Icarus* 66:117–124.
Kirchner H. P. 1964. The thermal expansion of ceramic crystals. *Progress in Solid State Chemistry* 1:1–36.
Kittel C. 1996. *Introduction to solid state physics*, 7th ed. New York: John Wiley & Sons. 688 p.
Kittel C. and Kroemer H. 1980. *Thermal physics*, 2nd ed. New York: W. H. Freeman and Company. 473 p.
Kroeger F. R. and Swenson C. A. 1977. Absolute linear thermal-expansion measurements on copper and aluminum from 5 to 320 K. *Journal of Applied Physics* 48:853–862.
Lagerros J. S. V. 1996. Thermal physics of asteroids I. Effects of shape, heat conduction and beaming. *Astronomy & Astrophysics* 310:1011–1020.
Lashley J. C., Hundley M. F., Migliori A., Sarrao J. L., Pagliuso P. G., Darling T. W., Jaime M., Cooley J. C., Hults W. L., Morales L., Thoma D. J., Smith J. L., Boerio-Goates J., Woodfield B. F., Stewart G. R., Fisher R. A., and Phillips N. E. 2003. Critical examination of heat capacity measurements made on a quantum design physical property measurement system. *Cryogenics* 43:369–378.
Levy R. A. 1968. *Principles of solid state physics*. New York: Academic Press. 474 p.
Loehle S., Jenniskens P., Böhrk H., Bauer T., Elsäer H., Sears D. W., Zolensky M. E., and Shaddad M. H. 2017. Thermophysical properties of Almahata Sitta meteorites (asteroid 2008 TC3) for high-fidelity entry modeling. *Meteoritics & Planetary Science* 52:197–205.
Łuszczek K. and Wach R. A. 2014. NWA 6255 meteorite—Thermophysical properties of interior and the crust. *Meteorites* 3:33–44.
Macke R. J. 2010. Survey of meteorite physical properties: Density, porosity and magnetic susceptibility. PhD thesis, University of Central Florida, USA.
Macke R. J., Consolmagno G. J., and Britt D. T. 2011. Density, porosity, and magnetic susceptibility of carbonaceous chondrites. *Meteoritics & Planetary Science* 46:1842–1862.
Macke R. J., Opeil C., and Consolmagno G. J. 2019. Heat capacities of ordinary chondrite falls below 300 K. *Meteoritics & Planetary Science* 54:2729–2743.
Marinkovic B. A., Jardim P. M., Saavedra A., Lau L. Y., Baehtz C., de Avillez R. R., and Rizzo F. 2004. Negative thermal expansion in hydrated HZSM-5 orthorhombic zeolite. *Microporous and Mesoporous Materials* 71:117–124.
Matsui T. and Osako M. 1979. Thermal properties of yamato meteorites. *Memoirs of the National Institute Of Polar Research, Special Issue* 15:243–252.
McAdam M. M., Sunshine J. M., Howard K. T., and McCoy T. M. 2015. Aqueous alteration on asteroids: Linking the mineralogy and spectroscopy of CM and CI chondrites. *Icarus* 245:320–332.
McSween H. Y. Jr. 1979. Are carbonaceous chondrites primitive or processed? A review. *Reviews of Geophysics and Space Physics* 17:1059–1078.
McSween H. Y. Jr. 1987. Aqueous alteration in carbonaceous chondrites: Mass balance constraints on matrix mineralogy. *Geochemica et Cosmochimica Acta* 51:2469–2477.
Miller W., Smith C. W., Mackenzie D. S., and Evans K. E. 2009. Negative thermal expansion: A review. *Journal of Material Science* 44:5441–5451.
Moin P. B. 2013. Second-order phase transitions and Ehrenfest equation for strained solids. *Philosophical Magazine* 93:4593–4597.
Molaro J. L., Byrne S., and Lec J.-L. 2017. Thermally induced stresses in boulders on airless body surfaces, and implications for rock breakdown. *Icarus* 294:247–261.
Moore D. F. and Geyer W. 1974. A review of hysteresis theories for elastomers. *Wear* 30:1–34.
Müller T. G., Sterzik M. F., Schütz O., Pravec P., and Siebenmorgen R. 2004. Thermal infrared observations of near-Earth asteroid 2002 NY40*. *Astronomy & Astrophysics* 424:1075–1080.
Opeil C. P., Consolmagno G. J., and Britt D. T. 2010. The thermal conductivity of meteorites: New measurements and analysis. *Icarus* 208:449–454.
Opeil C. P., Consolmagno G. J., Safarik D. J., and Britt D. T. 2012. Stony meteorite thermal properties and their relationship with meteorite chemical and physical states. *Meteoritics & Planetary Science* 47:319–329.
Pertermann M. and Hofmeister A. M. 2006. Thermal diffusivity of olivine-group minerals at high temperature. *American Mineralogist* 91:1747–1760.
Putzig N. E., Mellon M. T., Kretke K. A., and Arvidson R. E. 2005. Global thermal inertia and surface properties of Mars from the MGS mapping mission. *Icarus* 173:325–341.
Rao C. N. R. and Rao G. V. S. 1970. Electrical conduction in metal oxides. *Physica Status Solidi A* 1:597–651.
Ravaji B., Ali-Lagoa V., Delbó M., and Wilkerson J. W. 2019. Unraveling the mechanics of thermal stress weathering: Rate-effects, size-effects, and scaling laws. *Journal of Geophysics Research* 124:3304–3328.
Rosenberg H. M. 1992. *The solid state*. Oxford: Oxford University Press. 326 p.
Rubin A. E., Trigo-Rodriguez J. M., Huber H., and Wasson J. T. 2007. Progressive aqueous alteration of CM carbonaceous chondrites. *Geochimica et Cosmochimica Acta* 71:2361–2382.
Sakatani N., Ogawa K., Iijima Y., Arakawa M., Honda R., and Tanaka S. 2017. Thermal conductivity model for powdered materials under vacuum based on experimental studies. *AIP Advances* 7:015310.
Sass J. H., Lachenbruch A. H., and Munroe R. J. 1971. Thermal conductivity of rocks from measurements on fragments and its application to heat-flow determination. *Journal Geophysical Research* 76:3391–3401.
Schmiedeshoff G. M., Lounsbury A. W., Luna D. J., Tracy S. J., Schramm A. J., Tozer S. W., Correa V. F., Hannahs S. T., Murphy T. P., Palm E. C., Lacerda A. H., Bud'ko S. L., Canfield P. C., Smith J. L., Lashley J. C., and Cooley J. C. 2006. Versatile and compact capacitive dilatometer. *Review of Scientific Instruments* 77:123907/1–123907/8.
Shomate C. H. 1954. A method for evaluating and correlating thermodynamic data. *Journal of Physical Chemistry* 58:368–372.

Stachurski Z. H. 2011. On structure and properties of amorphous materials. *Materials* 4:1564–1598.

Takenaka K. 2012. Negative thermal expansion materials: Technological key for control of thermal expansion. *Science and Technology of Advanced Materials* 13:013001.

Takenaka K. and Takagi H. 2005. Giant negative thermal expansion in Ge-doped anti-perovskite manganese nitrides. *Applied Physics Letters* 87:261902/1–261902/3.

Turton R. 2005. *The physics of solids*. Oxford: Oxford University Press. 432 p.

Velbel M. A., Tonui E. K., and Zolensky M. E. 2012. Replacement of olivine by serpentine in the carbonaceous chondrite Nogoya (CM2). *Geochimica et Cosmochimica Acta* 87:117–135.

Vokrouhlický D., Bottke W. F., Chesley S. R., Scheeres D. J., Statler T. S. 2015. The Yarkovsky and YORP effects. In *Asteroids IV*, edited by Michel P. Tucson, Arizona: University of Arizona Press. pp. 509–531.

Vosteen H.-D. and Schellschmidt R. 2003. Influence of temperature on thermal conductivity, thermal capacity and thermal diffusivity for different types of rock. *Physics and Chemistry of the Earth* 28:499–509.

Vu T. H., Piqueux S., Choukroun M., Edwards C. S., Christensen P. R., and Glotch T. D. 2019. Low-temperature specific heat capacity measurements and application to Mars thermal modeling. *Icarus* 321:824–840.

Waples D. W. and Waples J. S. 2004. A review and evaluation of specific heat capacities of rocks, minerals, and subsurface fluids. Part 1: Minerals and nonporous rocks. *Natural Resources Research* 13:97–121.

Weisberg M. K., McCoy T. J., Krot A. N. 2006. Systematics and evaluation of meteorite classification meteorites and the early solar system II. In *Meteorites and the early solar system II*, edited by Lauretta D. S. and McSween H. T. Jr. Tuscon, Arizona: University of Arizona Press. pp. 19–52.

Whittington A. G., Hofmeister A. M., and Nabelek P. I. 2009. Temperature-dependent thermal diffusivity of the Earth's crust and implications for magmatism. *Nature* 458:319–321.

Wood J. A. 1967. Chondrites: Their metallic minerals, thermal histories, and parent planets. *Icarus* 6:1–49.

Xiong Z. and Zhang B. 2019. Thermal transport properties of olivine, wadsleyite, and ringwoodite—A review. *Minerals* 9:519.

Zhang Z., Thiéry M., and Baroghel-Bouny V. 2014. A review and statistical study of existing hysteresis models for cementitious materials. *Cement and Concrete Research* 57:44–60.

Zolensky M. E., Mittlefehldt D. W., Lipschutz M. E., Wang-Sheng M., Clayton R. N., Mayeda T. K., Grady M. M., Pillinger C., and Barber D. 1997. CM chondrites exhibit the complete petrologic range from type 2 to 1. *Geochimica et Cosmochimica Acta* 61:5099–5115.